GDCh Research Article Angewandte International Edition Chemie www.angewandte.org

How to cite: *Angew. Chem. Int. Ed.* **2025**, e202513552
doi.org/10.1002/anie.202513552

Photochemistry

Photo-Induced Catalytic Dearomative Coupling of *N*-Heteroarenes

Fan Lin, Ting-Ting Song, Yan Liu, Xiao-Yu Wang, Shi-Yu Guo, Yaguang Sun,* and Qing-An Chen**

Abstract: Naturally occurring dimeric products have attracted considerable attention from both chemists and pharmacologists. The construction of pseudo-dimers often requires elaborate synthetic effort with low efficiency. Dearomatization reactions represent an ideal method to transform planar aromatics into 3D skeletons, which has attracted increasing interest in medicinal chemistry and total synthesis. Herein, we present a dearomative dimerization of *N*-heteroarenes under mild photochemical conditions. Through additive regulation, the catalytic dearomative cross-coupling of two distinct quinolines could also be achieved. With aromatic compounds as coupling partners, this strategy provides a straightforward avenue to pseudo-dimers of *N*-heteroarenes. Combined experimental and computational mechanistic studies reveal the intertwined EnT/SET nature and offered guidelines for synthesizing novel bridged polycycles. In addition, this strategy provides an effective approach for constructing functional polymers with high atom economy and environmental benefits via metal-free, one-pot polymerization. Furthermore, the synthetic transformations offer a complementary route to access formal crossed products that were previously inaccessible.

Introduction

Dimeric natural products comprise a class of metabolites with diverse structures and bioactivities, attracting growing interest from synthetic and biological researchers.[1–5] Over the past few decades, numerous dimers derived from common natural product families have been identified, such as the dimers of alkaloids,[6] xanthanolide,[7] and terpenoids.[8] Current synthetic methods for dimeric natural products primarily involve conjugate additions, radical reactions, esterifications, (cross) coupling reactions, and cycloaddition/oxidative cyclization.[9,10] However, the synthesis of unsymmetrical dimeric products typically demands more elaborate strategies compared to their symmetrical counterparts. Thus, developing a mild and simple method for constructing unsymmetrical dimers is highly desirable.

Aromatic molecules constitute one of the most fundamental and abundant classes of organic compounds, which are widely used in various fields of molecular science. Not surprisingly, the chemistry of these molecules is a vibrant field characterized by their unique reactivity patterns and inherent stability. High electronic stabilization renders the aromatic ring inert to many common chemical transformations, which can be divided into two categories by whether the aromaticity is destroyed or not (Figure 1a). The aromatic substitution reaction, including *ipso* substitution[11–14] and non-*ipso* substitution (C─H functionalization)[15–19] is one of the most widely applied reaction classes in pharmaceutical and chemical research, providing a broadly useful platform for the modification of aromatic ring scaffolds. The dehydrogenative dimerization is an efficient method to deliver the biphenyl dimerization moiety.[20–22] In contrast to direct functionalization, dearomatization reactions generate reactive intermediates to enable rapid access to structurally complex, value-added, and synthetically versatile 3D molecules from arene feedstocks.[23–29] Besides classical hydrogenation-based strategies,[30,31] only a limited range of reagents are capable of initiating dearomatization through nucleophilic addition (typically reduction) or photo-induced radical addition.[32–35]

In this context, photo-induced energy transfer strategies can enable impressive reactivity modes.[36–39] Among them, as efficient chemical processes, dearomative cycloadditions demonstrate stereospecificity, atom economy, and the ability to achieve molecular complexity in one step.[27,29,40] Glorius et al. have successfully developed photocatalytic dearomatization using a series of nonaromatic partners (such as alkenes and bicyclo[1.1.0]butanes) to construct various attractive polycyclic compounds (Figure 1b).[41–44] Due to the unique reactivity and inherent stability of aromatic compounds, dearomatization reactions using aromatic partners remain highly challenging. Only photodimerization of anthracenes under high-energy ultraviolet irradiation were reported.[45–48] Taking advantage of intramolecular reaction manner, You and other groups have developed photo-induced intramolecular double dearomative cycloaddition of indole derivatives

[*] F. Lin, Y. Sun
Shenyang University of Chemical Technology, Shenyang 110142, China
E-mail: sunyaguang@syuct.edu.cn

F. Lin, T.-T. Song, Y. Liu, X.-Y. Wang, S.-Y. Guo, Q.-A. Chen
Dalian Institute of Chemical Physics, Chinese Academy of Sciences, 457 Zhongshan Road, Dalian 116023, China
E-mail: ttsong@dicp.ac.cn
qachen@dicp.ac.cn

Y. Liu, X.-Y. Wang, Q.-A. Chen
University of Chinese Academy of Sciences, Beijing 100049, China

Additional supporting information can be found online in the Supporting Information section

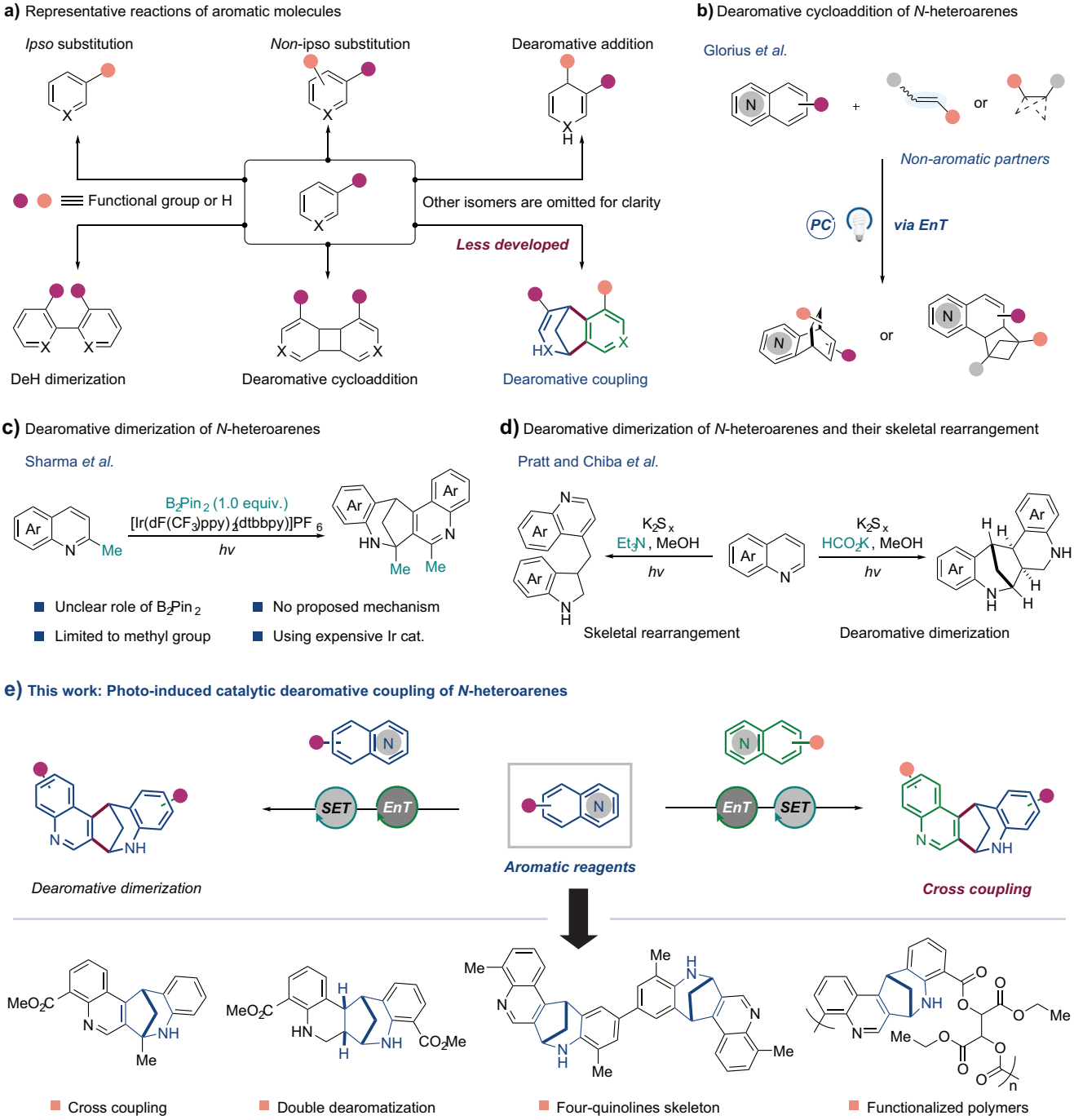

Figure 1. Divergent transformations of *N*-heteroarenes. a) Representative reactions of aromatic molecules. b) Dearomative cycloaddition of *N*-heteroarenes. c) Dearomative dimerization of *N*-heteroarenes. d) Dearomative dimerization of *N*-heteroarenes and their skeletal rearrangement. e) This work: Photo-induced catalytic dearomative coupling of *N*-heteroarenes.

bearing a pendant aromatic ring.[49,50] Although the pioneering work on iridium-based photocatalytic intermolecular unsymmetrical coupling of 2-methyl quinolines was reported by Sharma et al. (Figure 1c), use of expensive Ir catalyst and stoichiometric amount of B_2pin_2, narrow substrate scope with 2-position blocked, and obscure mechanism hampered the development of this method.[51] During the revision of this manuscript, Pratt and Chiba et al. demonstrated the reductant-regulated divergent transformations of quinolines using polysulfide anions as photocatalysts (Figure 1d).[52] However, limitations in substrate scope and stereoselectivity issues continue to restrict the broader utility of this approach. Moreover, more challenging dearomative cross-coupling of two different quinolines could not be achieved in the above two protocols.

Inspired by these precedents and based on our research interests in olefin functionalizations[53–58] and photocatalytic dearomatization,[59–61] we herein present a photo-induced

dearomative coupling of simple quinolines to construct pyridine-fused polycyclic rings in one step under metal-free conditions (Figure 1e).[62] Particularly, the cross-coupling reactions of two different quinolines could be achieved through additive regulation. Combined experimental and computational mechanistic studies revealed the intertwined EnT/SET process and offered guidelines for designing new bridged polycyclic molecules. Of particular note, multi-functional polymers and formal crossed products could be accessed directly or via simple transformations.

Reaction Optimization

We commenced our studies using 8-methoxy quinoline **1a** as the model substrate to optimize the reaction (Figure 2). First, as state-of-the-art energy transfer-mediated dearomative photocycloaddition of *N*-heteroarenes, Glorius' elegant protocols[41,43] were applied to this substrate. All results demonstrated that no detectable pseudo-dimeric product **2** was formed under Glorius' conditions (entries 1–3). The combination of **PC-II** and B_2Pin_2[51] gave **2** in a low yield (entry 4). As shown in the bar charts at the top of Figure 2, a range of reaction conditions were investigated. TFA was found to be the superior additive through the evaluation of different Lewis and Brønsted acids. In addition, the solvent has a significant effect on the dearomatization reaction. No reaction occurred in trifluoroethanol (TFE) or dichloromethane (DCM). And *N*,*N*-dimethylacetamide (DMAc) emerged as the optimal solvent. The loading effect investigation suggested 1.5 equiv of TFA was the best. These screening studies revealed that product **2** could be regioselectively prepared in good yield by catalysis with thioxanthone as photocatalyst (5 mol%), TFA as additive in DMAc (entry 5). Photosensitizer $[Ir(dF(CF_3)ppy)_2(dtbbpy)]PF_6$ (**PC-II**) proved to be less efficient (entry 6). Interestingly, the desired product **2** was obtained with 21% yield with TFA alone (entry 7). However, no product formation was observed in the absence of acid or light (entries 8 and 9). The thermal conditions (70 °C) did not promote the reaction (entry 10). A low yield was obtained under air conditions (entry 11). For methyl 8-quinoline carboxylate (**1f**), photosensitizer 5CzBN (**PC-III**) was identified as the optimal photocatalyst, providing **7** in 95% yield (Table S6, entry 4). Both the acid and solvent systems demonstrated significant influence on the formation of **7** (Tables S7 and S8). TFA and DMSO were found to be the superior additive and solvent. An additive-based screening[63] was subsequently performed to assess the functional group tolerance, displaying a good tolerance for unprotected alcohols, halides, and diverse heterocyclic compounds. Conversely, basic amine functionalities and alkenes seemed to inhibit product formation (Table S19).

Substrate Scope Investigation

With optimal conditions established, we then moved to investigate the scope of *N*-heteroarenes bearing diverse functional groups such as aryl, alkyl, alkenyl, heterocyclic, and ester groups. Pleasingly, a variety of functional groups were well tolerated, thus highlighting the accessibility to a broad library of pyridine-fused polycyclic products (Figure 3). First, variations of the electron-rich substituents (—Me, —OMe, and —Ph) at the 8-position of the quinoline ring were examined. The corresponding pseudo-dimers (**2**–**4**) could be obtained in decent yields. The structure of **3** has been further confirmed by single crystal X-ray crystallography (CCDC: 2344938).[64] Gratifyingly, thiophenyl and furanyl groups at the 8-position of the quinoline ring were also compatible to give corresponding products **5** and **6**. Then, the applicability of *N*-heteroarenes bearing various electron-withdrawing groups (—CO_2R, —COR, —CN, and —X) at the 8-position was further investigated. Aromatic substrates with diverse ester substituents, including those containing alkyl (**1f**, **1h**, and **1i**), alkenyl (**1g**), and fluoroalkyl (**1k**) moieties, all performed well under the optimized conditions, delivering polycyclic products **7**–**13** in 41%–81% yields. The structure of **7** has been further confirmed by single crystal X-ray crystallography (CCDC: 2344939).2 To our delight, **14** and **15** bearing −COMe and −CN substituents could also be obtained in reasonable yields. Substrates bearing halogen groups (—F, —Cl, and —Br) proved effective substrates, affording the desired dimers **16**–**18** in decent yields (71%–74%). Moreover, 7-quinoline carboxylate (**1r**) and 7-chloroquinoline (**1s**) proved amenable to this dearomative coupling reaction (**19** and **20**). Substrate **1t** bearing electron-rich substituent (—Me) at the 7-position of the quinoline could also be tolerated. Notably, —Me and —Cl substituents at the 6-position of the quinoline were also applicable in this protocol, affording the desired products (**22** and **23**). Furthermore, 2-substituted quinolines performed well to deliver bridged products (**24**–**27**) in 38%–62% yields. Simple quinoline and *o*-phenanthroline also worked smoothly thus providing polycyclized products **28** and **29**. The structure of **29** has been further confirmed by single crystal X-ray crystallography (CCDC: 2344946).[64] Some unsuccessful substrates, such as pyridines, isoquinolines, and indoles, are shown in Figure S3.

Various monomers bearing two quinolines with different linkers were prepared and applied to this protocol to construct functional polymers (Figure 4). The electron-deficient monomers were able to react smoothly, producing polymers **P1–P3** with satisfactory M_ws (up to 48.9 kg mol^{-1}) and relatively low dispersities (M_w/M_n = 1.14–1.55) in good yields. In addition, **P1–P3** showed good solubilities in common polar organic solvents such as DMF, DMSO, DMAc, DCM, and tetrahydrofuran (THF). It is worth noting that the polymer **P4** could also be obtained from the electron-rich monomer containing the alkoxy group in comparable yield with decent M_w (0.96 kg mol^{-1}) and low dispersity index (M_w/M_n = 1.27). Of note, **P4** exhibited slightly poor solubility in THF, probably due to the rigid structure of the connected benzene ring. This dearomatization strategy therefore proved to be a powerful tool for constructing ring-fused heterocyclic polymers.

Thermal Stability. The thermal stability of **P1–P4** was evaluated by thermogravimetric analysis (TGA). As shown in Figure 4I, the decomposition temperatures (T_ds) of **P1–P4** at 5 wt% weight loss under nitrogen were 203–300 °C, suggesting their high thermal resistance. The glass transition

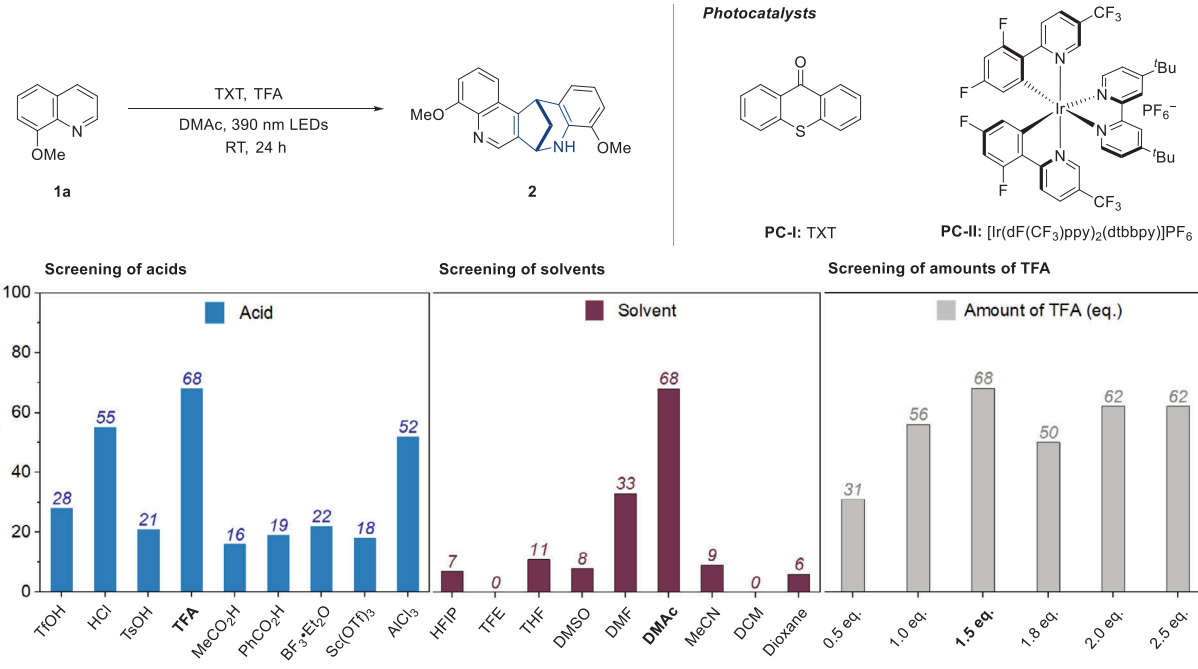

Entry	Variation from the standard conditions	Yield[a)] [%]
1	**PC-II** (2 mol%), HFIP[14a]	0
2	**PC-II** (1 mol%), $BF_3{\cdot}Et_2O$ (1.25 eq.), DCM[14a]	0
3	**PC-II** (2 mol%), HCl (2.0 eq.), HFIP[14c]	0
4	**PC-II** (1 mol%), B_2pin_2 (1.0 eq.), 1,4-Dioxane[17]	9
5	None	**68**
6	**PC-II** instead of **PC-I**	42
7	Without **PC-I**	21
8	Without TFA	0
9	Without light	0
10	Oil bath at 70 °C in the dark	0
11	Air instead of N_2	23

Figure 2. Optimization of the reaction conditions. Standard conditions: **1a** (0.10 mmol), TFA (1.5 equiv), TXT (5 mol%), DMAc (1.0 mL), 390 nm LEDs, RT, 24 h. [a)]Yields were determined by GC-FID using mesitylene as the internal standard.

temperatures (T_gs) of the polymers were also measured by differential scanning calorimetry, and the T_gs of **P1–P4** were found to be 61, 150, 152, and 59 °C, respectively (Figures S33D–36D). Therefore, the good thermal stability of these polymers with different morphologies endows them with application potential as carbon materials.

Photophysical Properties. Figure 4II shows the UV absorption spectra of synthesized polyquinolines in THF. The spectra of **P1–P3** exhibited a strong absorption in the range of 330–405 nm with a maximum peak at 381, 374, and 370 nm, respectively. No obvious absorption peak was observed in the range of 330–405 nm for **P4**, while only at 298 nm. The photoluminescence (PL) spectra of polyquinolines in THF are shown in Figure 4III. Upon photoexcitation, polymers **P1–P4** exhibited emission peaks centered at 480, 470, 476, and 484 nm, respectively.

Optimization and Substrate Scope for Cross-Coupling

After realizing homo coupling of quinolines, we investigated whether this catalytic protocol is suitable for dearomative cross-coupling between different quinolines (Figure 5a). First, we investigated the homo coupling of substrate **1b** and **1ag** under different acidic conditions, respectively (Tables S11 and S12). The results showed that TFA promoted the dimerization of **1b** but suppressed that of **1ag**. Instead, substrate **1ag** exhibited higher reactivity under weaker acidic conditions

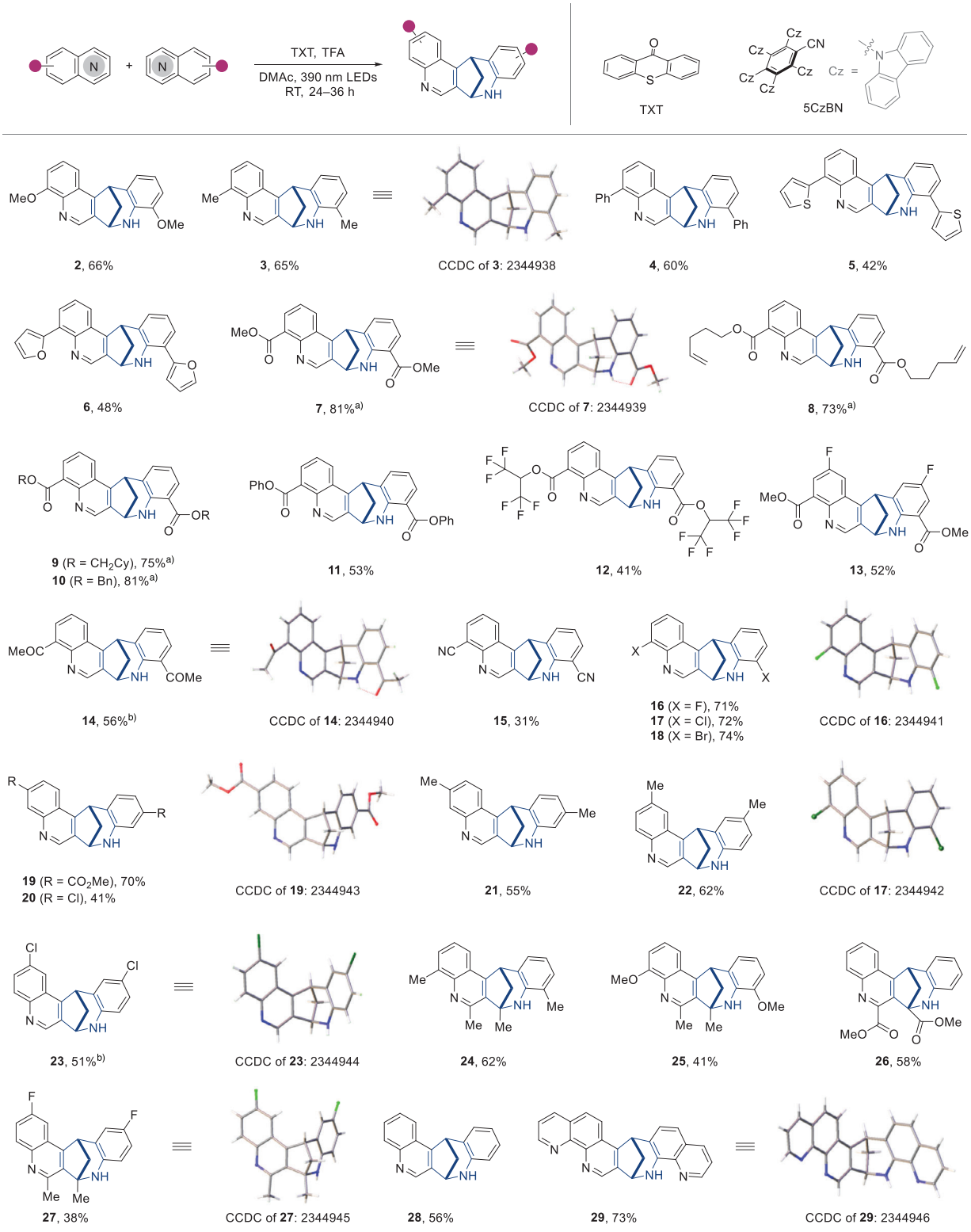

Figure 3. Substrate scope of the dimerization illustrated with various *N*-heteroarenes. Reaction conditions: **1** (0.40 mmol), TFA (1.5 equiv), TXT (5 mol%), DMAc (2.0 mL), 390 nm LEDs, RT, 24–36 h. [a] 5CzBN (1 mol%) was used instead of TXT, and DMSO was used as solvent. [b] HOAc was used instead of TFA.

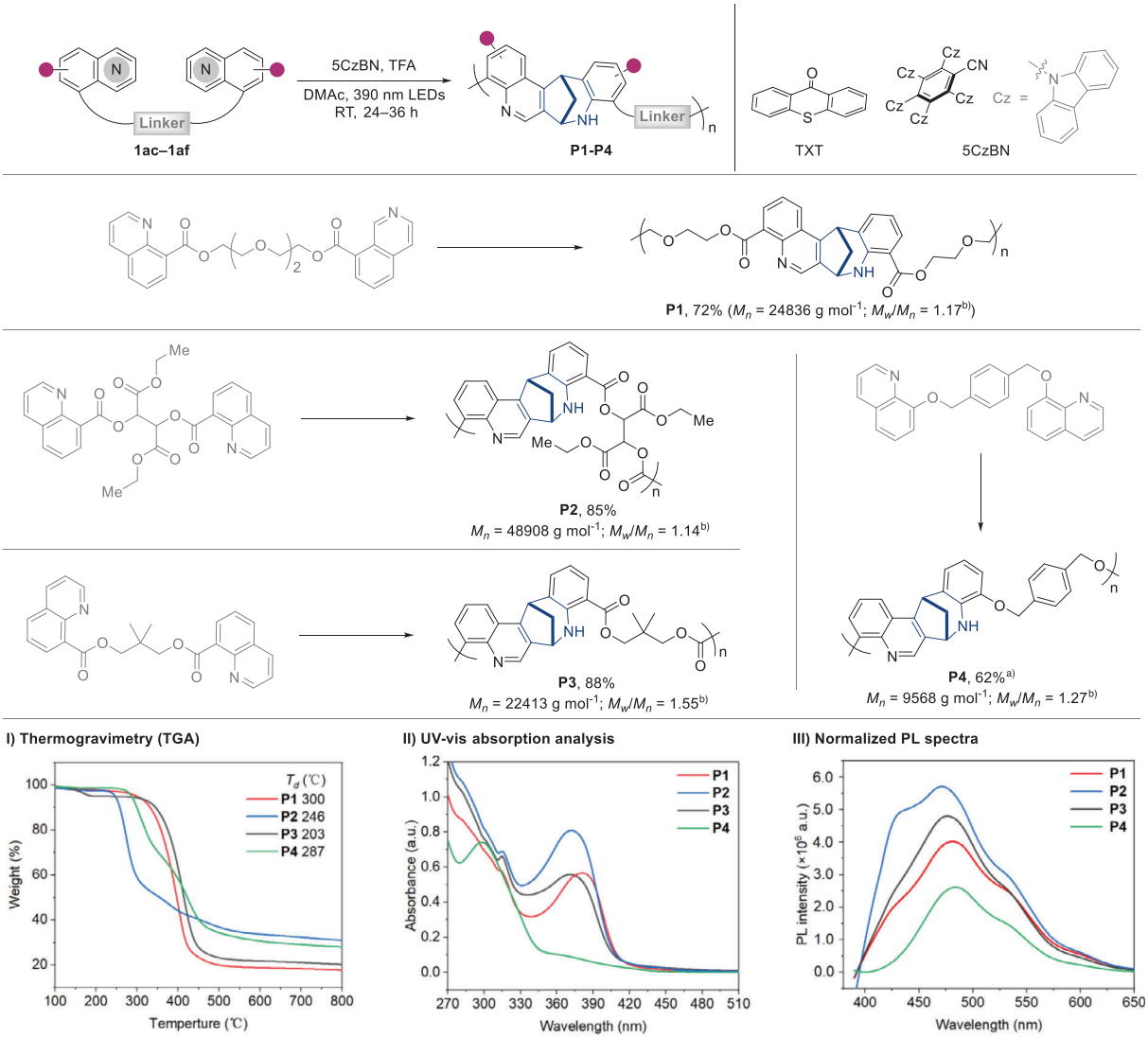

Figure 4. Substrate scope. Multifunctional polymers. (I) Thermogravimetry. (II) UV–vis absorption analysis. (III) Normalized PL spectra. Conditions: **1** (0.40 mmol), TFA (1.5 equiv), 5CzBN (1 mol%), DMSO (2.0 mL), 390 nm LEDs, RT, 24–36 h. [a] TXT (5 mol%) was used instead of 5CzBN, DMAc was used as solvent. [b] Determined by GPC in THF using a linear polystyrene as calibration standard.

(HOAc). Furthermore, a screening of acid was subsequently performed to evaluate the cross-coupling studies between 8-methylquinoline (**1b**) and 2-methylquinoline (**1ag**) (Table S13). In the presence of 5CzBN and TFA, the reaction gave the target products **30** and **30′** in 5% and 5% yields, respectively (entry 1). Encouragingly, when weaker acid HCO_2H or HOAc was added, the yield of **30** was increased to 36% or 53% (entries 2 and 3). However, Lewis acid ($BF_3{\cdot}Et_2O$) failed to effectively promote this transformation (entry 4). 5CzBN was found to be optimal through the evaluation of different photocatalysts (Table S14). The polysulfide anion photocatalyst developed by Chiba and coworkers was also investigated.[52] However, no (crossed) dimerization product formation was observed (entry 6). Given the observation of the self-polymerization byproducts during the reaction process, the ratio of the starting materials was adjusted (entries 7 and 8). When the ratio of **1b**/**1ag** was changed to 1:3, a higher yield (74%) was obtained (entry 8). A slightly increased yield was achieved when the catalyst loading was increased to 4 mol% (entry 9). Notably, this transformation did not proceed in the absence of acidic conditions (entry 10).

With the optimized conditions in hand, the substrate scope for cross-coupling reactions between different quinoline molecules was explored (Figure 5b). First, model product **30** was obtained in 82% isolated yield, whose structure was verified by single crystal X-ray crystallography (CCDC: 2415017).[64] When using 8-methyl quinoline (**1b**) as aromatic coupling partner, quinolines bearing various functionalities at the C6, C7, and C8 positions could be converted into the corresponding dearomative cross-coupling products **30**–**36** in good yields. In addition to 8-Me quinoline, quinolines with different substituents (—OMe, —Cl, and —Me) were also applied to this transformation as coupling partners to undergo dearomatizative cross-coupling of 2-methyl quinoline, delivering polycyclic products **37**–**40** in 65%–74% yields. Upon activation of $PhCO_2H$, the quinoline with an ester

a) **Optimization for dearomative cross-coupling of quinolines**

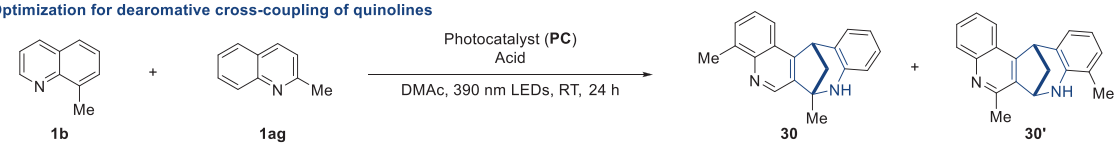

Entry	**1b** (eq.)	**1ag** (eq.)	**PC** (mol%)	Acid (eq.)	Yield (%)	
					30	**30'**
1	1.0	1.0	5CzBN (2)	TFA (1.5)	5	5
2	1.0	1.0	5CzBN (2)	HCO_2H (1.5)	36	3
3	1.0	1.0	5CzBN (2)	HOAc (1.5)	53	4
4	1.0	1.0	5CzBN (2)	$BF_3{\cdot}Et_2O$ (1.5)	8	9
5	1.0	1.0	TXT (10)	HOAc (1.5)	13	2
6	1.0	1.0	K_2S_x (10 mol%/S)	HOAc (1.5)	0	0
7	1.0	2.0	5CzBN (2)	HOAc (1.5)	67	7
8	1.0	3.0	5CzBN (2)	HOAc (1.5)	74	4
9	1.0	3.0	5CzBN (4)	HOAc (1.5)	**83**	3
10	1.0	3.0	5CzBN (4)	--	0	0

Reactions were performed on a 0.10 mmol scale. Yields were determined by GC-FID using mesitylene as the internal standard.

b) **Substrate scope for dearomative cross-coupling of quinolines**

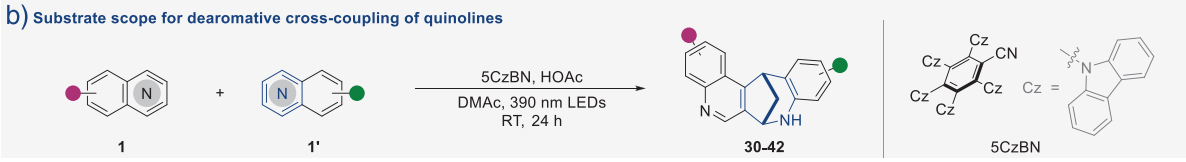

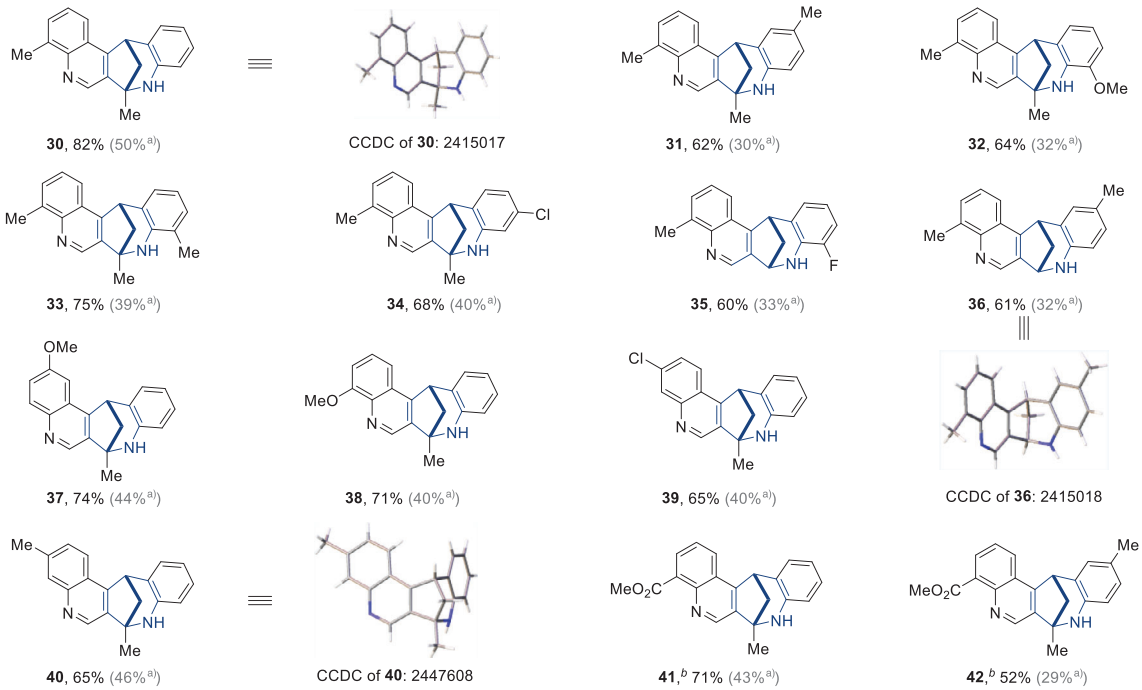

Figure 5. Catalytic dearomative cross-coupling of quinolines. a) Optimization for dearomative cross-coupling of quinolines; b) Substrate scope for dearomative cross-coupling of quinolines. Reaction conditions: **1** (0.20 mmol), **1'** (0.60 mmol), 5CzBN (4 mol%), HOAc (1.5 equiv), DMAc (1.0 mL), 390 nm LEDs, RT, 24 h. [a] **1'** (0.2 mmol) was used. [b] $PhCO_2H$ (1.5 equiv) was used instead of HOAc.

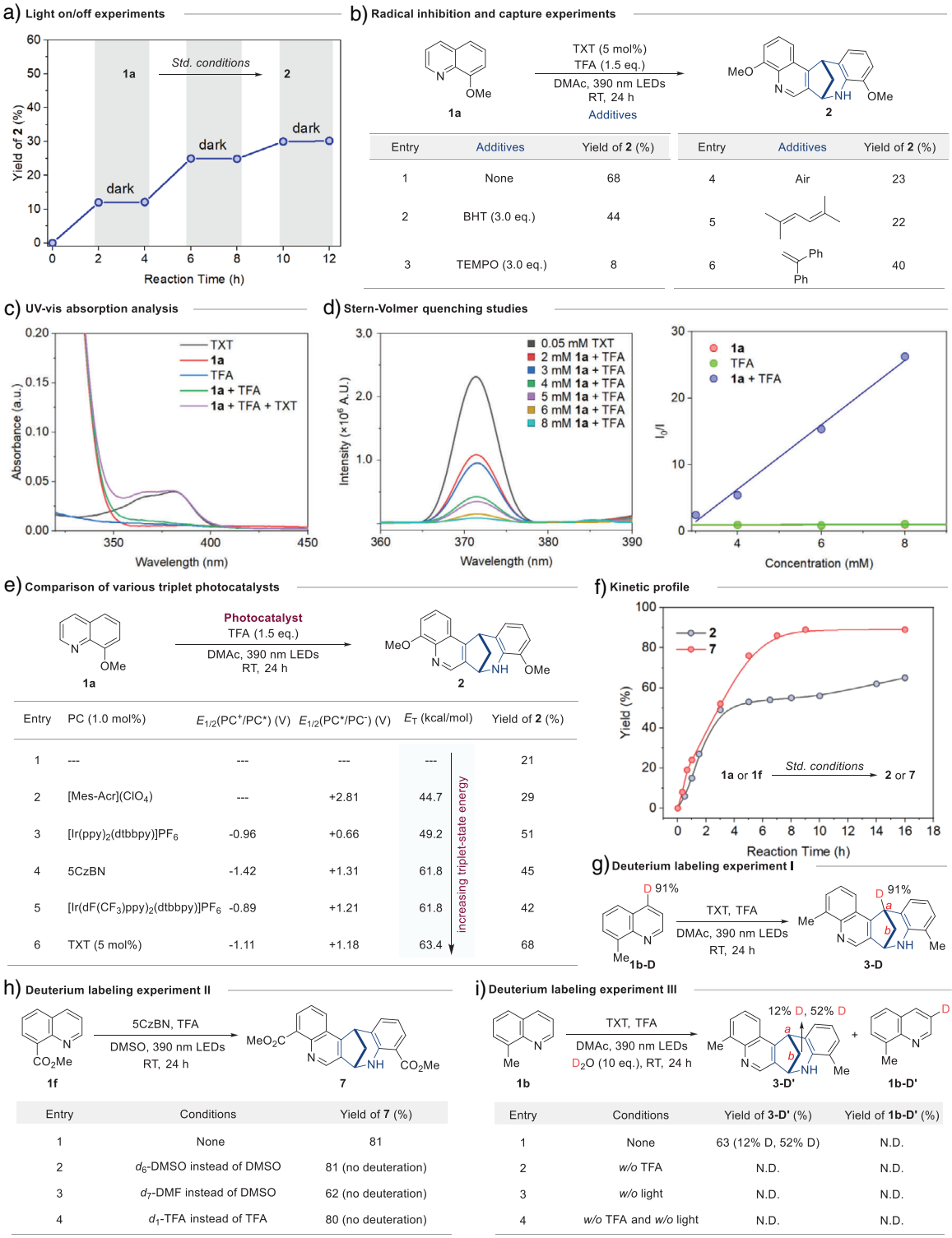

Entry	Additives	Yield of **2** (%)	Entry	Additives	Yield of **2** (%)
1	None	68	4	Air	23
2	BHT (3.0 eq.)	44	5		22
3	TEMPO (3.0 eq.)	8	6		40

Entry	PC (1.0 mol%)	$E_{1/2}(PC^+/PC^*)$ (V)	$E_{1/2}(PC^*/PC^-)$ (V)	E_T (kcal/mol)	Yield of **2** (%)
1	---	---	---	---	21
2	[Mes-Acr](ClO_4)	---	+2.81	44.7	29
3	$[Ir(ppy)_2(dtbbpy)]PF_6$	-0.96	+0.66	49.2	51
4	5CzBN	-1.42	+1.31	61.8	45
5	$[Ir(dF(CF_3)ppy)_2(dtbbpy)]PF_6$	-0.89	+1.21	61.8	42
6	TXT (5 mol%)	-1.11	+1.18	63.4	68

Entry	Conditions	Yield of **7** (%)
1	None	81
2	d_6-DMSO instead of DMSO	81 (no deuteration)
3	d_7-DMF instead of DMSO	62 (no deuteration)
4	d_1-TFA instead of TFA	80 (no deuteration)

Entry	Conditions	Yield of **3-D'** (%)	Yield of **1b-D'** (%)
1	None	63 (12% D, 52% D)	N.D.
2	*w/o* TFA	N.D.	N.D.
3	*w/o* light	N.D.	N.D.
4	*w/o* TFA and *w/o* light	N.D.	N.D.

Figure 6. Mechanistic studies. a) Light on/off experiments. b) Radical inhibition and capture experiments. c) UV–vis absorption analysis. d) Stern–Volmer quenching studies. e) Comparison of various triplet photocatalysts. f) Kinetic profile. g–i) Deuterium-labeling experiments.

group could also act as an aromatic coupling partner in cross-coupling to afford products **41** and **42** in reasonable yields. When investigating the 1:1 ratio of substrates, we observed reduced cross-product yields, highlighting the importance of reactant stoichiometry. The yields of the corresponding homo dimers were included in Figure S12, while the applicability of this cross-coupling reaction was summarized in Figure S13. In conclusion, under weakly acidic conditions, quinolines substituted at the 6-, 7-, or 8-position more readily serve as aromatic coupling partners to disrupt the aromaticity of quinoline substrates bearing weakly electron-donating substituents.

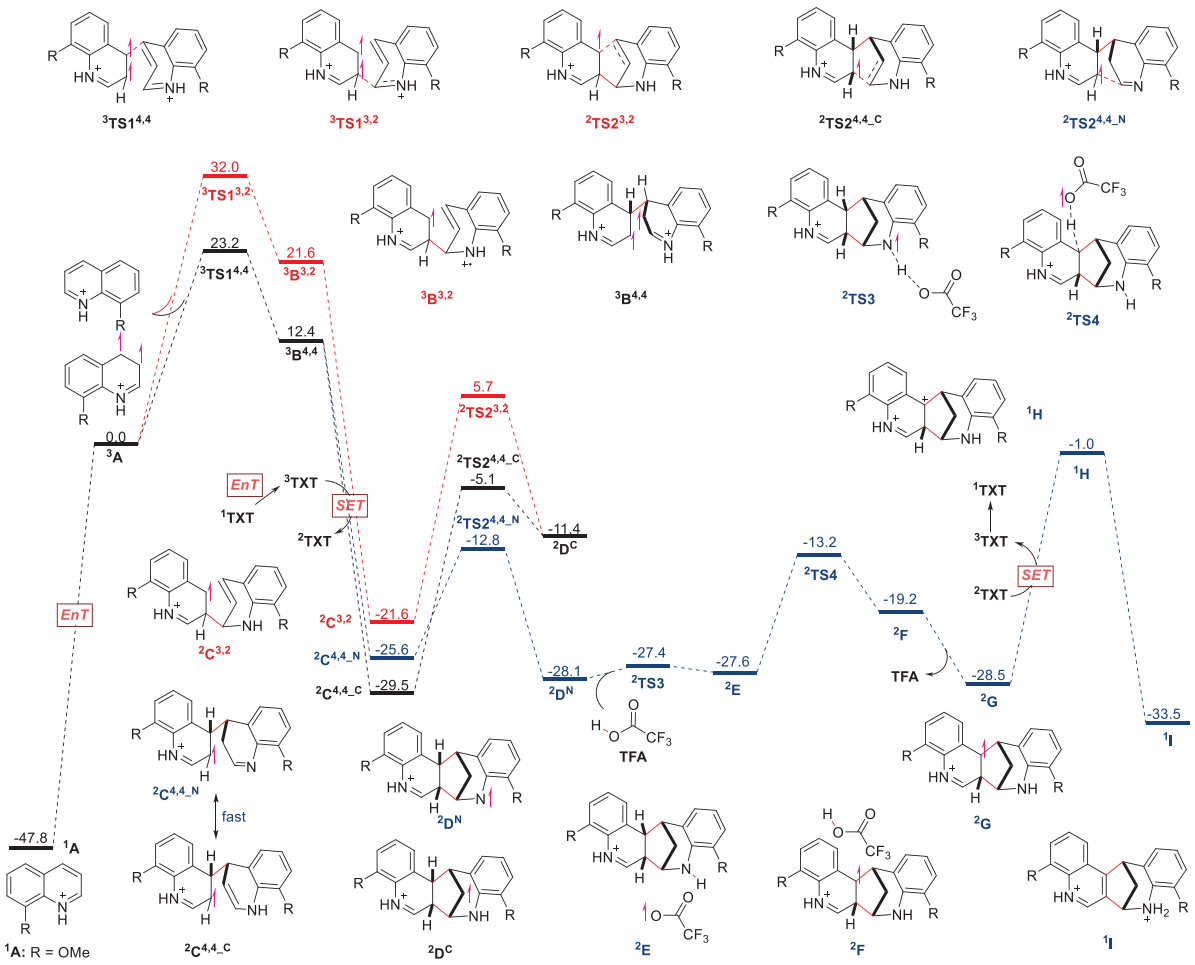

Figure 7. Calculated energy diagram for photo-induced dearomative coupling of *N*-heteroarenes.

Mechanistic Investigation

To shed light on our mechanistic hypothesis, a series of mechanistic experiments were conducted (Figure 6). First, light on/off experiments showed that the transformation was interrupted in the absence of light, thus suggesting the crucial role of light irradiation and ruling out a long radical chain process (Figure 6a). Second, the dearomative process was suppressed when adding radical inhibitor TEMPO or BHT (Figure 6b, entries 1–3), which hints the radical nature of the reaction. On the other hand, the standard reaction was significantly inhibited in the presence of known triplet quenchers, such as O_2, 2,5-dimethylhexa-2,4-diene, or 1,1-diphenylethylene (Figure 6b, entries 4–6). It suggests the involvement of excited triplet-state intermediates in this dearomative coupling process. Next, the photocatalyst thioxanthone (TXT) was found to be the only light-absorbing species in the reaction near the excitation wavelength (λ_{max} = 390 nm) from ultraviolet–visible (UV–vis) absorption spectroscopy (Figure 6c). Then, a Stern–Volmer analysis revealed that the luminescence emission of thioxanthone was quenched efficiently by [**1a** + TFA] mixture, whereas no quenching was observed with **1a**, which indicates that an interaction between thioxanthone and [**1a** + TFA] existed in the reaction medium (Figure 6d). To understand the nature of their interaction, the comparison of a series of photocatalysts with different properties was conducted (Figure 6e). As a result, no obvious linear correlation between the yield of **2** and the triplet energy was observed. Moreover, the kinetic profile of a standard reaction mixture of **1a** (**1f**) with TFA showed that the reaction proceeded very fast and did not have obvious induction periods, with the majority of the product formed within 6 h (Figure 6f). Meanwhile, substrate **1f** showed higher reactivity than **1a**.

A series of deuterium-labeling experiments were performed using deuterated quinoline or deuterated reagents under standard conditions (Figures 6g–i). When using deuterated quinoline at the 4 position (**1b-D**) as the starting material, the deuterium atom at *a* position was retained, and no deuterium incorporation onto other positions of the obtained deuterated product **3-D** was observed (Figure 6g). Next, several deuterated reagents (d_6-DMSO, d_7-DMF, d_1-TFA) were used under standard conditions, and no deuterium incorporation was observed in product **7** (Figure 6h). These results implied that *N*-centered radical ^{2}**D^N** is more likely to be the intermediate participating in the HAT process, rather than radical ^{2}**D^C** (see the DFT in Figure 7). When an additional 10 equiv deuterium water was added into the

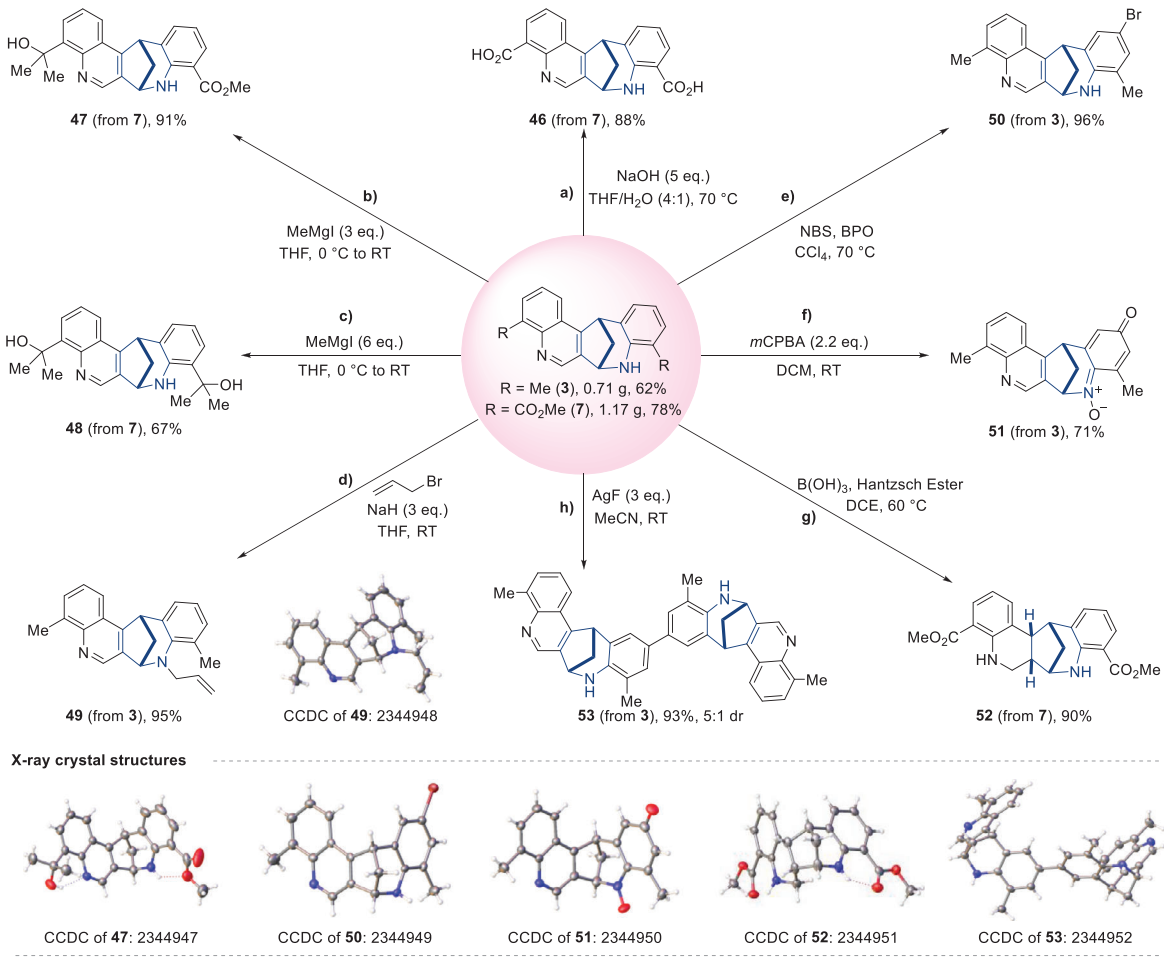

Figure 8. Synthetic transformations. a) **7** (0.10 mmol), NaOH (5 eq.), THF/H_2O (1.0 mL, 4/1), 70 °C, 12 h; b) **7** (0.10 mmol), MeMgI (3 eq.), THF (1.0 mL), 0 °C to RT, 18 h; c) **7** (0.10 mmol), MeMgI (6 eq.), THF (1.0 mL), 0 °C to RT, 24 h; d) **3** (0.10 mmol), 3-bromopropene (2 eq.), NaH (3 eq.), THF (1.0 mL), RT, 12 h; e) **3** (0.10 mmol), NBS (1.0 eq.), BPO (2 mol%), CCl_4 (0.5 mL), 70 °C, 12 h; f) **3** (0.10 mmol), *m*CPBA (2.2 eq.), DCM (1.0 mL), RT, 12 h; g) **7** (0.10 mmol), $B(OH)_3$ (15 mol%), Hantzsch Ester (3 eq.), DCE (1.0 mL), 60 °C, 16 h; h) **3** (0.10 mmol), AgF (3 eq.), MeCN (1.0 mL), RT, 8 h.

reaction system of substrate **1b**, and obvious deuterations of both *b* bridge-position (12% D and 52% D) were incorporated in the obtained product **3D'** (Figure 6i). To rule out the possibility of the formation of **3D'** from **1b-D'**, a series of control experiments were carried out. No product (**3D'** or **1b-D'**) was observed in the absence of TFA or light (entries 2–4), which indicated that a fast proton exchange might be involved during the formation of some key intermediates.

For the cross-coupling reaction (Figure 5), the addition of acids significantly influenced both the reaction efficiency and selectivity, underscoring their pivotal role. Based on this observation, we hypothesized that the acid additives were binding to the quinolines through acid-base interactions, as previously reported.[41–44] To probe the interaction between the excited photosensitizer (5CzBN*) and protonated quinolines, Stern–Volmer luminescence quenching experiments were conducted (Figures S27 and S28). The results showed that protonated quinolines (**1b** and **1ag**, treated with TFA or HOAc) effectively quenched the excited state of 5CzBN*. However, no consistent positive correlation was observed between the quenching efficiency and the reaction yield. This discrepancy suggests that the photosensitizer plays multiple roles in the reaction system—instead, a more intricate mechanism involving an intertwined EnT/SET pathway may be involved. Furthermore, the kinetic profiles of the **1b**/**1ag** cross-coupling reaction revealed distinct product distributions under different acid conditions (Figure S27). TFA promoted preferential formation of the homo dimer **3**, while HOAc converted the selectivity toward the cross-coupling product **30**, despite inevitable formation of homo dimer **43**.

Based on the aforementioned mechanistic studies and further DFT calculations, a plausible mechanism is proposed as outlined (Figure 7). Visible light excitation of the photocatalyst yields an excited state complex which sensitizes the protonated quinoline ^{1}**A** via an EnT process. Given the computed spin densities on C2, C3, and C4 of ^{1}**A** are 0.259, 0.037, and 0.483, respectively, the resulting triplet quinoline species ^{3}**A** favors the addition onto C4 with protonated quinoline ^{1}**A** (Figure S58). Through transition state ^{3}**TS1**,[4,4] diradical ^{3}**A** attacks protonated quinoline ^{1}**A** to produce a 1,4-triplet diradical ^{3}**B**.[4,4] DFT calculations also predict that kinetically unfavorable 3,2′-radical addition between ^{1}**A** and ^{3}**A** needs to overcome a higher free energy barrier, 32.0 kcal mol^{-1} (via ^{3}**TS1**^{3,2}) compared to 4,4′-radical addition

with 23.2 kcal mol^{-1} (via ^{3}**TS1**^{4,4}). The photoexcited species ^{3}**TXT** undergoes a single-electron oxidation by the resulting diradical ^{3}**B**^{4,4} to deliver radical cation ^{2}**TXT** and radical intermediate ^{2}**C**$^{4,4\text{-N}}$. During this process, rapid isomerization occurs between ^{2}**C**$^{4,4\text{-N}}$ and ^{2}**C**$^{4,4\text{-C}}$. Then, ^{2}**C**$^{4,4\text{-N}}$ undergoes intramolecular radical addition to deliver *N*-centered radical ^{2}**D**^{N} via transition state ^{2}**TS2**$^{4,4\text{-N}}$ with an activation free energy of 12.8 kcal mol^{-1}. This process determines the stereoselectivity. However, the other two pathways (via ^{2}**TS2**^{3,2} or ^{2}**TS2**$^{4,4\text{-C}}$) will need to overcome the higher free energy barriers (>30 kcal mol^{-1}) to give carbon-centered radical ^{2}**D**^{C}. Then, TFA engages in hydrogen atom abstraction (HAA)[65–67] through transition state ^{2}**TS3** to give radical intermediate ^{2}**E**. A second HAA occurs subsequently to form a benzyl radical ^{2}**F**. Further dissociation of TFA produces radical intermediate ^{2}**G**, which can be oxidized by ^{2}**TXT** to form corresponding cation ^{1}**H** and simultaneously regenerates the photocatalyst. Finally, a deprotonative aromatization of ^{1}**H** delivers the thermodynamically favorable product ^{1}**I**.

Synthetic Transformations

To further demonstrate the synthetic potential of this protocol, scale-up reactions and further synthetic transformations have been performed. As shown in Figure 8, pyridine-fused polycyclic rings **3** (0.71 g) and **7** (1.17 g) have been prepared in scale-up experiments with 62% and 78% yield, respectively. Basic hydrolysis of **7** afforded carboxylic acid **46** in good yield. Based on the addition of amounts of Grignard reagents, compound **7** reacted with 3.0 equiv or 6.0 equiv of MeMgI, affording **47** or **48** with one or two sterically encumbered tertiary alcohols in 91% and 67% yield, respectively. The structure of **47** was further confirmed by single crystal X-ray crystallography (CCDC: 2344947).[64] In addition, the allyl-protected tertiary amine **49** was obtained from secondary amine **3** in excellent yield. Moreover, compound **3** could be further selectively brominated by NBS to deliver brominated product **50** in excellent yield, which provides a supplement for the synthesis of formal crossed products that were previously inaccessible. Noteworthy, by treating **3** with *m*CPBA, a dearomatized cyclohexadienone imide *N*-oxide **51** was isolated in decent yield instead of a simple *N*-oxide. Furthermore, product **7** could be selectively hydrogenated in the presence of Hantzsch ester to give hydrogenated product **52** in high yield.[68] The structures of **49**–**53** have been further confirmed by single crystal X-ray crystallography (CCDC: 2344948–2344952).[64] Interestingly, an oxidative coupling of **3** in MeCN promoted by AgF gave smooth entry into benzidine **53** bearing a four-quinoline-linked skeleton in excellent yield, which enables the leap from dimerization to tetramerization. Overall, this dearomative coupling strategy could provide direct and efficient access to various functionalized bridged polycycles.

Conclusion

In conclusion, we have developed a visible-light-induced dearomative dimerization of *N*-heteroarenes via an intertwined EnT/SET pathway, which allowed the facile synthesis of highly pyridine-fused bridged polycyclic scaffolds. By the regulation of additives, the catalytic dearomative cross-coupling of two different quinolines could also be realized. This strategy provides a straightforward avenue to pseudo-dimers of *N*-heteroarenes using both aromatic compounds as coupling partners. Furthermore, the construction of functional polymers with unique architectures by this metal-free visible light-mediated photocatalysis unlocks a novel synthetic route to polyquinolines. We anticipate this work will find substantial application in accelerating the development of ring-fused heterocyclic compounds and polymer materials in future research.

Acknowledgements

The authors thank Prof. Zhi-Shi Ye (DUT) for helpful discussions and manuscript revisions. Generous financial support from the Dalian Institute of Chemical Physics (DICPI201902) and the National Natural Science Foundation of China (22371275 and 22071239) is acknowledged.

Conflict of Interests

The authors declare no conflict of interest.

Data Availability Statement

The X-ray crystallographic data for compounds have been deposited in the Cambridge Crystallographic Data Centre (CCDC). All other data are available in the Supporting Information.

Keywords: Cross-coupling · Dearomatization · Dimers, *N*-heteroarenes · Photocatalysis

[1] G. Bérubé, *Curr. Med. Chem.* **2006**, *13*, 131.
[2] M. Vrettou, A. A. Gray, A. R. E. Brewer, A. G. M. Barrett, *Tetrahedron* **2007**, *63*, 1487–1536.
[3] S. A. Snyder, A. M. ElSohly, F. Kontes, *Nat. Prod. Rep.* **2011**, *28*, 897.
[4] J. Sun, H. Yang, W. Tang, *Chem. Soc. Rev.* **2021**, *50*, 2320–2336.
[5] Y. Fan, J. Shen, Z. Liu, K. Xia, W. Zhu, P. Fu, *Nat. Prod. Rep.* **2022**, *39*, 1305–1324.
[6] V. G. Lisnyak, T. C. Sherwood, S. A. Snyder, *Acc. Chem. Res.* **2021**, *54*, 1610–1622.
[7] H. Shang, J. Liu, R. Bao, Y. Cao, K. Zhao, C. Xiao, B. Zhou, L. Hu, Y. Tang, *Angew. Chem. Int. Ed.* **2014**, *53*, 14494–14498.
[8] Y. Chang, C. Sun, C. Wang, X. Huo, W. Zhao, X. Ma, *Nat. Prod. Rep.* **2022**, *39*, 2030–2056.
[9] H. Oikawa, T. Tokiwano, *Nat. Prod. Rep.* **2004**, *21*, 321–352.
[10] G. Lian, B. Yu, *Chem. Biodivers.* **2010**, *7*, 2660.
[11] J. G. Traynham, *Chem. Rev.* **1979**, *79*, 323–330.
[12] M. Tiecco, *Acc. Chem. Res.* **1980**, *13*, 51–57.
[13] S. M. Bonesi, M. Fagnoni, *Chem. Eur. J.* **2010**, *16*, 13572–13589.

[14] F. Sandfort, T. Knecht, T. Pinkert, C. G. Daniliuc, F. Glorius, *J. Am. Chem. Soc.* **2020**, *142*, 6913–6919.
[15] K. Murakami, S. Yamada, T. Kaneda, K. Itami, *Chem. Rev.* **2017**, *117*, 9302–9332.
[16] S. C. Fosu, C. M. Hambira, A. D. Chen, J. R. Fuchs, D. A. Nagib, *Chem* **2019**, *5*, 417.
[17] R. S. J. Proctor, R. J. Phipps, *Angew. Chem. Int. Ed.* **2019**, *58*, 13666–13699.
[18] N. Holmberg-Douglas, D. A. Nicewicz, *Chem. Rev.* **2022**, *122*, 1925–2016.
[19] B. Zhao, B. Prabagar, Z. Shi, *Chem* **2021**, *7*, 2585–2634.
[20] S. H. Cho, J. Y. Kim, J. Kwak, S. Chang, *Chem. Soc. Rev.* **2011**, *40*, 5068.
[21] F. Lv, Z.-J. Yao, *Sci. China Chem.* **2017**, *60*, 701–720.
[22] M. C. Carson, M. C. Kozlowski, *Nat. Prod. Rep.* **2024**, *41*, 208–227.
[23] C. J. Huck, D. Sarlah, *Chem* **2020**, *6*, 1589.
[24] M. Okumura, D. Sarlah, *Eur. J. Org. Chem.* **2020**, *2020*, 1259–1273.
[25] Y.-Z. Cheng, Z. Feng, X. Zhang, S.-L. You, *Chem. Soc. Rev.* **2022**, *51*, 2145–2170.
[26] C. J. Huck, Y. D. Boyko, D. Sarlah, *Nat. Prod. Rep.* **2022**, *39*, 2231.
[27] M. Zhu, X. Zhang, C. Zheng, S.-L. You, *Acc. Chem. Res.* **2022**, *55*, 2510–2525.
[28] D.-H. Liu, J. Ma, *Angew. Chem. Int. Ed.* **2024**, *63*, e202402819.
[29] P. Ji, K. Duan, M. Li, Z. Wang, X. Meng, Y. Zhang, W. Wang, *Chem. Soc. Rev.* **2024**, *53*, 6600–6624.
[30] D.-S. Wang, Q.-A. Chen, S.-M. Lu, Y.-G. Zhou, *Chem. Rev.* **2012**, *112*, 2557–2590.
[31] M. P. Wiesenfeldt, Z. Nairoukh, T. Dalton, F. Glorius, *Angew. Chem. Int. Ed.* **2019**, *58*, 10460–10476.
[32] F. López Ortiz, M. J. Iglesias, I. Fernández, C. M. Andújar Sánchez, G. Ruiz Gómez, *Chem. Rev.* **2007**, *107*, 1580–1691.
[33] S. Park, S. Chang, *Angew. Chem. Int. Ed.* **2017**, *56*, 7720–7738.
[34] N. Kratena, B. Marinic, T. J. Donohoe, *Chem. Sci.* **2022**, *13*, 14213–14225.
[35] M. Escolano, D. Gaviña, G. Alzuet-Piña, S. Díaz-Oltra, M. Sánchez-Roselló, C. d. Pozo, *Chem. Rev.* **2024**, *124*, 1122–1246.
[36] F. Strieth-Kalthoff, M. J. James, M. Teders, L. Pitzer, F. Glorius, *Chem. Soc. Rev.* **2018**, *47*, 7190–7202.
[37] Q. Q. Zhou, Y. Q. Zou, L. Q. Lu, W. J. Xiao, *Angew. Chem. Int. Ed.* **2019**, *58*, 1586–1604.
[38] J. Großkopf, T. Kratz, T. Rigotti, T. Bach, *Chem. Rev.* **2022**, *122*, 1626.
[39] S. Dutta, J. E. Erchinger, F. Strieth-Kalthoff, R. Kleinmans, F. Glorius, *Chem. Soc. Rev.* **2024**, *53*, 1068–1089.
[40] R. Remy, C. G. Bochet, *Chem. Rev.* **2016**, *116*, 9816–9849.
[41] J. Ma, S. Chen, P. Bellotti, R. Guo, F. Schäfer, A. Heusler, X. Zhang, C. Daniliuc, M. K. Brown, K. N. Houk, F. Glorius, *Science* **2021**, *371*, 1338–1345.
[42] R. Guo, S. Adak, P. Bellotti, X. Gao, W. W. Smith, S. N. Le, J. Ma, K. N. Houk, F. Glorius, S. Chen, M. K. Brown, *J. Am. Chem. Soc.* **2022**, *144*, 17680–17691.
[43] J. Ma, S. Chen, P. Bellotti, T. Wagener, C. Daniliuc, K. N. Houk, F. Glorius, *Nat. Catal.* **2022**, *5*, 405–413.
[44] R. Kleinmans, S. Dutta, K. Ozols, H. Shao, F. Schäfer, R. E. Thielemann, H. T. Chan, C. G. Daniliuc, K. N. Houk, F. Glorius, *J. Am. Chem. Soc.* **2023**, *145*, 12324–12332.
[45] H.-D. Becker, *Chem. Rev.* **1993**, *93*, 145–172.
[46] H. Bouas-Laurent, A. Castellan, J. P. Desvergne, R. Lapouyade, *Chem. Soc. Rev.* **2000**, *29*, 43–55.
[47] H. Bouas-Laurent, J.-P. Desvergne, A. Castellan, R. Lapouyade, *Chem. Soc. Rev.* **2001**, *30*, 248–263.
[48] J. Wesemann, P. G. Jones, D. Schomburg, L. Heuer, R. Schmutzler, *Chem. Ber.* **1992**, *125*, 2187–2197.
[49] M. Zhu, H. Xu, X. Zhang, C. Zheng, S. L. You, *Angew. Chem. Int. Ed.* **2021**, *60*, 7036–7040.
[50] G. Zhen, G. Zeng, K. Jiang, F. Wang, X. Cao, B. Yin, *Chem. Eur. J.* **2023**, *29*, e202203217.
[51] I. Kumar, S. S. Gupta, R. Kumar, R. Kumar, P. Agrawal, D. Sahal, U. Sharma, *ACS Sustain. Chem. Eng.* **2020**, *8*, 12902–12910.
[52] E. Y. K. Tan, A. Dehdari, A. S. Mat Lani, D. A. Pratt, S. Chiba, *Chem* **2024**, *10*, 3722–3734.
[53] Y.-C. Hu, D.-W. Ji, C.-Y. Zhao, H. Zheng, Q.-A. Chen, *Angew. Chem. Int. Ed.* **2019**, *58*, 5438–5442.
[54] C.-S. Kuai, D.-W. Ji, C.-Y. Zhao, H. Liu, Y.-C. Hu, Q.-A. Chen, *Angew. Chem. Int. Ed.* **2020**, *59*, 19115–19120.
[55] S.-Y. Guo, F. Yang, T.-T. Song, Y.-Q. Guan, X.-T. Min, D.-W. Ji, Y.-C. Hu, Q.-A. Chen, *Nat. Commun.* **2021**, *12*, 6538.
[56] W.-S. Jiang, D.-W. Ji, W.-S. Zhang, G. Zhang, X.-T. Min, Y.-C. Hu, X.-L. Jiang, Q.-A. Chen, *Angew. Chem. Int. Ed.* **2021**, *60*, 8321–8328.
[57] X. Huang, B.-Z. Chen, P. Li, D.-W. Ji, J. Liu, H. Zheng, S.-N. Yang, Y.-C. Hu, B. Wan, X.-P. Hu, C. Fu, Y. Huang, J. Zheng, Q.-A. Chen, S. Ma, *Nat. Chem.* **2022**, *14*, 1185–1192.
[58] G. Zhang, C.-Y. Zhao, X.-T. Min, Y. Li, X.-X. Zhang, H. Liu, D.-W. Ji, Y.-C. Hu, Q.-A. Chen, *Nat. Catal.* **2022**, *5*, 708–715.
[59] T.-T. Song, Y.-K. Mei, Y. Liu, X.-Y. Wang, S.-Y. Guo, D.-W. Ji, B. Wan, W. Yuan, Q.-A. Chen, *Angew. Chem. Int. Ed.* **2024**, *63*, e202314304.
[60] T.-T. Song, F. Lin, S.-T. Xu, B.-C. Zhou, L.-M. Zhang, S.-Y. Guo, X. Zhang, Q.-A. Chen, *Angew. Chem. Int. Ed.* **2025**, *64*, e202505906.
[61] X.-X. Zhang, S.-T. Xu, X.-T. Li, T.-T. Song, D.-W. Ji, Q.-A. Chen, *J. Am. Chem. Soc.* **2025**, *147*, 11533–11542.
[62] T.-T. Song, F. Lin, Y. Liu, X.-Y. Wang, S.-Y. Guo, Y. Sun, Q.-A. Chen, *ChemRxiv* **2024**, doi: https://doi.org/10.26434/chemrxiv-2024-10dxt.
[63] K. D. Collins, F. Glorius, *Nat. Chem.* **2013**, *5*, 597–601.
[64] Deposition Numbers 2344938 (for **3**), 2344939 (for **7**), 2344940 (for **14**), 2344941 (for **16**), 2344942 (for **17**), 2344943 (for **19**), 2344944 (for **23**), 2344945 (for **27**), 2344946 (for **29**), 2415017 (for **30**), 2415018 (for **36**), 2447608 (for **40**), 2344947 (for **47**), 2344948 (for **49**), 2344949 (for **50**), 2344950 (for **51**), 2344951 (for **52**), and 2344952 (for **53**) contain the supplementary crystallographic data for this paper. These data are provided free of charge by the Cambridge Crystallographic Data Centre and Fachinformationszentrum Karlsruhe Access Structures service.
[65] N. Y. Shin, J. M. Ryss, X. Zhang, S. J. Miller, R. R. Knowles, *Science* **2019**, *366*, 364–369.
[66] E. Tsui, A. J. Metrano, Y. Tsuchiya, R. R. Knowles, *Angew. Chem. Int. Ed.* **2020**, *59*, 11845–11849.
[67] Y. Qin, Q. Zhu, R. Sun, J. M. Ganley, R. R. Knowles, D. G. Nocera, *J. Am. Chem. Soc.* **2021**, *143*, 10232–10242.
[68] D. Bhattacharyya, S. Nandi, P. Adhikari, B. K. Sarmah, M. Konwar, A. Das, *Org. Biomol. Chem.* **2020**, *18*, 1214–1220.

Manuscript received: June 20, 2025
Accepted manuscript online: July 14, 2025
Version of record online: ■■, ■■